Journal of Sound and Vibration (1999) **228**(4), 871–887
Article No. jsvi.1999.2452, available online at http://www.idealibrary.com on IDEAL®

DYNAMICAL BEHAVIOR OF FLYWHEEL ROTOR SUSPENDED BY HYSTERETIC FORCE OF HTSC MAGNETIC BEARING

TAKASHI HIKIHARA

School of Electrical Engineering, Kyoto University, Yoshida-honmachi, Sakyo, Kyoto 606-8501, *Japan*

HITOSHI ADACHI

Department of Electrical Engineering, Kansai University, Yamate-cho 3-3-35, *Suita, Osaka* 564-8680, *Japan*

FRANCIS C. MOON

Sibley School of Mechanical and Aerospace Engineering, Cornell University, Ithaca, New York 14853-7501, *U.S.A.*

AND

YOSHISUKE UEDA

School of Electrical Engineering, Kyoto University, Yoshida-honmachi, Sakyo, Kyoto 606-8501, *Japan*

(*Received* 6 *August* 1998, *and in final form* 11 *June* 1999)

Recently, the application of high-Tc superconductor to a magnetic bearing has reached the second stage in some institutes and companies. The static stability of the levitation has already been established. However, the dynamic stability is still under research because the non-linear magnetic characteristics of HTSC and the permanent magnet system are not sufficiently understood. In this paper, the dynamic behavior of a flywheel rotor suspended by HTSC magnetic bearing is discussed experimentally and numerically. The dynamics of the flywheel rotor shows an interesting gyroscopic motion under a hysteretic suspending force between HTSCs and permanent magnets. These types of dynamics have never been discussed before.

1. INTRODUCTION

Since the discovery of a high-Tc superconductor (HTSC), numerous applications have been proposed. Among them the superconducting magnetic bearing is one of the most possible applications of bulk HTSC and has been studied in many institutes and companies [1–3]. The development of the processing method of HTSC bulk, melt-powder melt-growth (MPMG), quench-melt-growth (QMG) and

0022–460X/99/490871 + 17 $30.00/0

so on, makes it possible to obtain the stable magnetic suspending force caused by its magnetic flux trapped in HTSC. In particular, it is widely recognized that its application to the flywheel energy storage system is highly advantageous in restricting energy loss through contact at the bearing.

The dynamics of the flywheel rotor suspended by a magnetic bearing shows the typical rigid-body dynamics described by classical mechanics. As for the rotor whose center of mass does not coincide with the center of horizontal force, the dynamic behavior becomes similar to a top. The imbalance of the rotor causes gyroscopic motion. These types of rotor dynamics suspended by a superconducting bearing have been studied by Harding [4, 5] and Bourke [6]. They identified the dynamical characteristics experimentally and clarified the low-energy dissipation characteristics.

The high-Tc superconducting magnetic bearing has a coupled structure of HTSCs and rare earth permanent magnets. The force–displacement relationship between the HTSC and the magnet has the hysteretic characteristics depending on the direction of relative displacement. Therefore, the dynamic behavior of the flywheel rotor suspended by the HTSC magnetic bearing is possibly affected by the non-linearity of the hysteretic force under the revolution. For example, the permanent magnet suspended by the HTSC magnetic bearing shows the lower and upper dirft of levitation under external disturbances [7–10]. The drift in mainly caused by the magnetic hysteretic characteristic. It was also confirmed by Coombs and Campbell [11] that the external vibration causes the gap decay of the HTSC flywheel system. Recently, we showed the drastic gap drift of the flywheel rotor suspended by the HTSC magnetic bearing at the resonant state under free revolution [12].

There are some models which can represent the hysteretic characteristics of the force–displacement relation [13–16]. It will be highly advantageous when it is substituted into the dynamic equations of the levitation system with the HTSC bearing. As for the rigid body suspended by HTSC magnetic bearings, both the vertical force–displacement hysteretic relationship and the lateral one have to be considered simultaneously in the dynamical equation. The dynamic behavior will show the gyroscopic motion. These types of motion under the hysteretic suspending force have never been discussed before. In this paper, we will discuss the dynamic behavior of a flywheel rotor suspended by HTSC magnetic bearing at a high revolution speed experimentally and numerically. Experimental results show the interesting and complex trajectories of the rotor behavior. It is also discussed that the experimental results can be numerically confirmed by using the former proposed mathematical models for hysteretic force–displacement relation.

2. EXPERIMENTAL SYSTEM AND SYSTEM SET-UP

2.1. FLYWHEEL SYSTEM WITH HTSC BEARING

The experimental system is shown in Figure 1. Four HTSC specimens are placed on the aluminium stage which keeps the temperature of HTSC specimens constant without soaking them in liquid nitrogen. The detailed dimension of the stage is given in Figure 2. The HTSC specimens are the MPMG processed $YBa_2Cu_3O_{7-x}$.

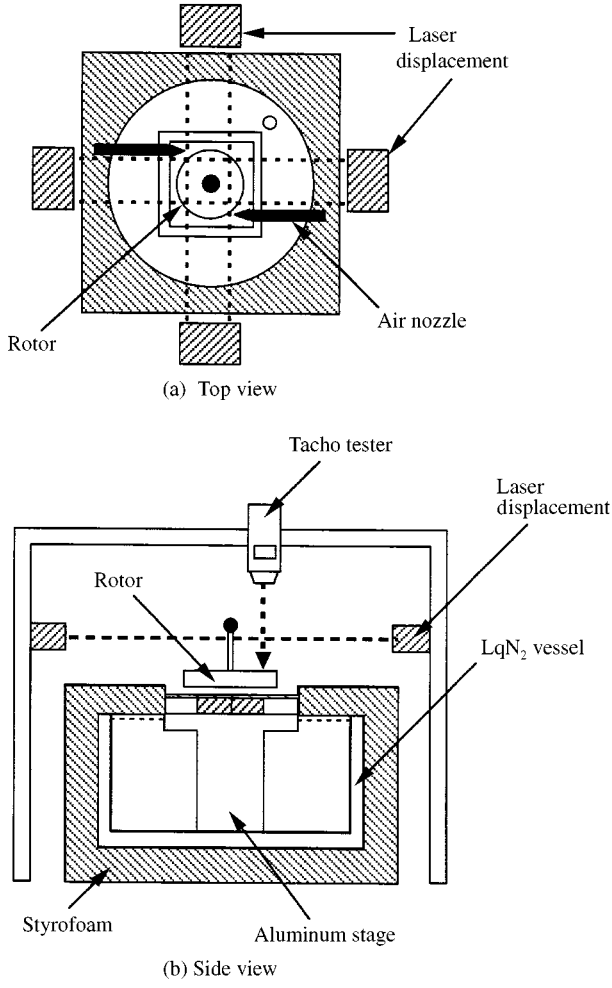

Figure 1. System configuration, (a) top view, and (b) side view.

The dimensions of the specimens are as follows: (1) specimen A: 42(L) × 42(W) × 15·5 (H) mm and 0·154 kg; (2) specimen B, 43 × 43 × 16 mm, 0·142 kg. The density of specimen B is lower than A. The surface of HTSC are covered by aluminum foil. A thin Styrofoam board is placed to keep the temperature of the HTSC surface constant. The thickness of the Styrofoam is 4·3 mm.

Figure 3 shows the structure and the dimension of the flywheel rotor. A ring-shaped permanent magnet is embedded at the bottom of the rotor composed of a cylindrical-shaped acrylic plastic. The permanent magnet is the NEOMAX-40, which has an outer diameter of ϕ 65 mm, an inner diameter of ϕ 35 mm and a height of 16 mm. The maximum flux density on the surface of the magnet of 0·4 T and the non-uniformity is less than 3·2% at 5·4 mm from the surface. In order to measure the dynamic behavior of the rotor, a shaft with a spherical marker is fixed on the vertical axis. The total weight of the rotor is 0·456 kg. A thin blade turbine with 8 wings is attached to the top surface of the rotor. The revolution of the

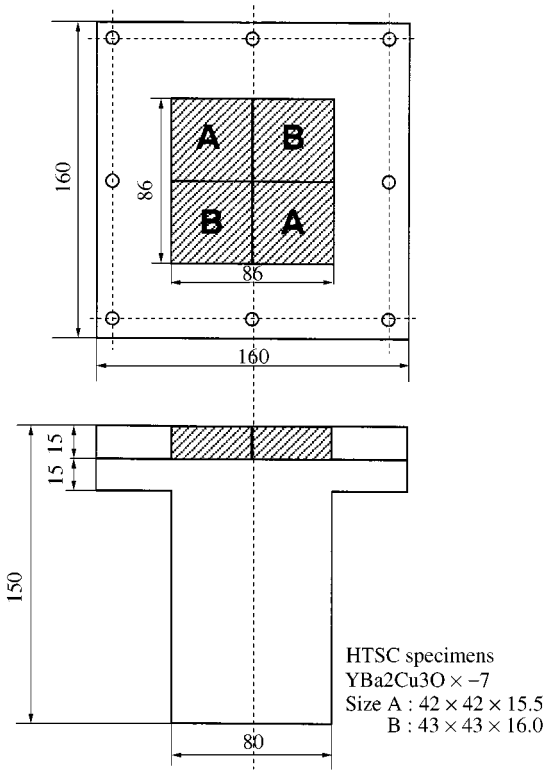

Figure 2. Stage for supporting and cooling HTSC specimens.

flywheel rotor is achived by blowing the compressed air against the turbine from the tangential direction through two nozzles.

2.2. MEASUREMENT SET-UP

In order to discuss the dynamic behaviour of the flywheel rotor under revolution, we need to detect the six degree of freedom as a rigid body. When the levitation of rotor is completely achieved, any contact-type displacement sensors and magnetic sensors must be avoided to exclude the damping force. Therefore, the displacement of the rotor is measured by two couples of laser displacement sensors (transmitter and detector), Keyence VG-035. They are set as shown in Figure 1(a). One couple of the sensors is arranged for estimating the x-axis displacement and another for the y-axis displacement. Figure 4(a) is the schematic diagram of the measurement set-up for the displacement. When the gyroscopic motion of the rotor appears, the shaft of the rotor moves in (x, y, z) space. However, we can neglect the z-axis displacement when the dynamic behavior of the whirling mode is discussed under high-speed revolution. The displacement (Δx, Δy) is equivalent to the horizontal x- and y-displacement as shown in Figure 4(b) respectively. They are also

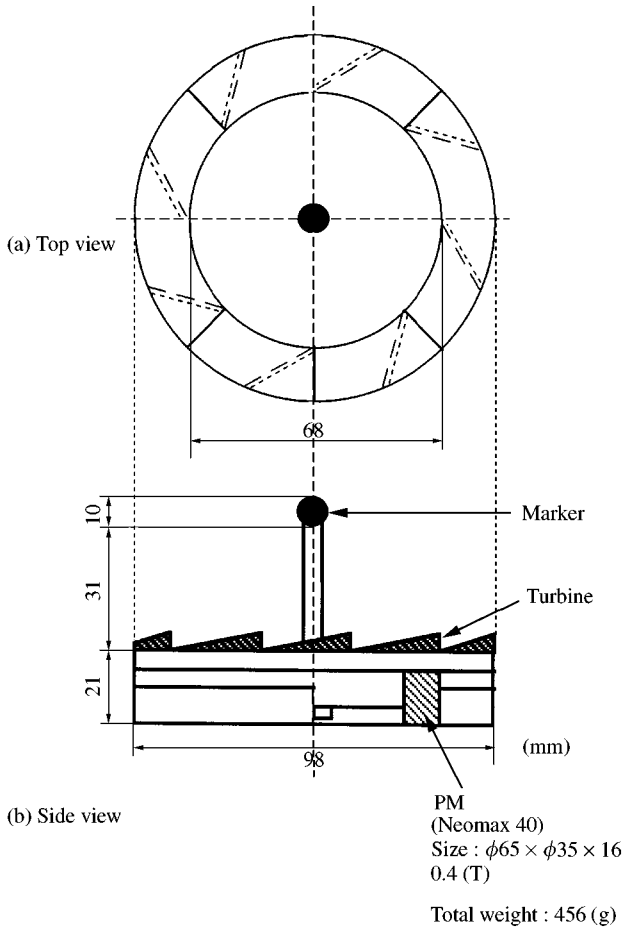

Figure 3. Structure and dimensions of flywheel rotor.

approximately equivalent to the angular displacement around the x- and y-axis respectively.

The revolution of the flywheel rotor is measured by a reflection-type tacho tester, HIOKI 3404. A reflective seal is attached to the surface of the rotor. The tester counts the reflection once in a revolution without any contact.

2.3. EXPERIMENTAL SET-UP

Experiments were performed as follows:

1. The flywheel rotor was set above the HTSC specimens by keeping the gap between the HTSC and the PM at 14·12 mm by a spacer. The revolution axis of the rotor was adjusted in a perpendicular direction at the center of the HTSC surface.

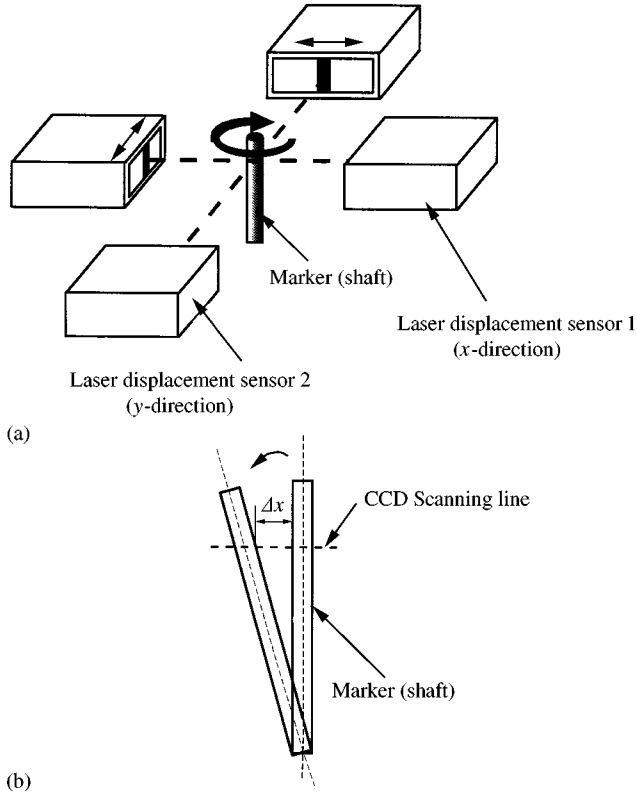

Figure 4. Schematic diagram for measurement of horizontal displacement, (a) set-up of laser displacement sensor and principle of measurement, (b) definition of displacement.

2. By keeping the gap between the HTSC and the PM, the HTSC specimens were cooled. (It is called "field cooling".) After the HTSCs showed the superconductivity completely, the spacer between the flywheel rotor and the HTSC was removed. Then the gap between them decreased until the levitation force achieved a balance to the weight of the flywheel. The rotor was magnetically suspended by the HTSC bearing without any contact.
3. The revolution of the flywheel rotor was accelerated by the compressed air blow gradually. When the revolution reached a desired speed, the air blow was stopped and the rotor fell into a free downward revolution mode.
4. During the free revolution, the horizontal x- and y-displacements were measured by two couples of laser displacement sensors until the revolution disappeared.

3. EXPERIMENTAL RESULTS

3.1. HYSTERETIC FORCE BETWEEN HTSC AND PERMANENT MAGNET

At first we will show the typical force-displacement characteristics between HTSC and PM. It is well-known that it has hysteretic characteristics depending

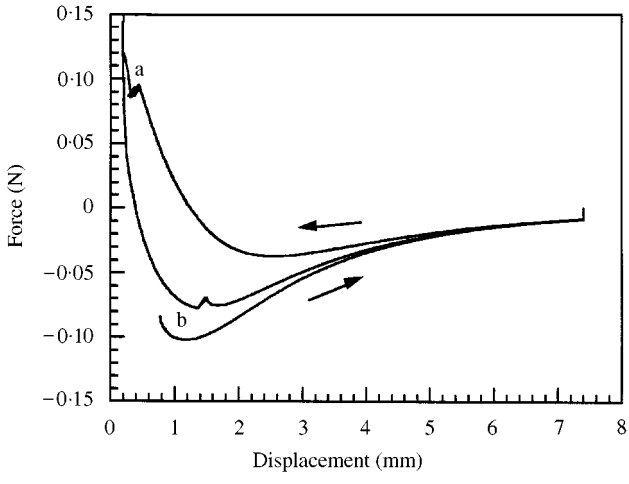

Figure 5. Vertical force–displacement characteristics with small perturbation test.

on its magnetic characteristics. The vertical force–displacement characteristics are shown in Figure 5 for a melt-quenched $YBa_2Cu_3O_{7-x}$ specimen [9] and the horizontal force–displacement characteristics in Figure 6 for a melt-powdered–melt-growth $YBa_2Cu_3O_{7-x}$ specimen [10]. As for the measurement system, the details are in references [9, 10]. In the process to measure hysteresis loops, the small perturbation was given in order to examine the dynamical stability of the equilibrium point at the steady state. Then the operating points showed the drift of the suspending force and the displacement towards the inside of the hysteresis loop. It is considered that the drift is caused by the creep of the flux trapped in HTSC.

3.2. DYNAMICAL BEHAVIOR OF FLYWHEEL ROTOR

In the experimental system, the flywheel can be spun up to around 12 000 r.p.m. The maximum revolution in the experimental system is limited by the capacity of the air-compressor to blow the air against the turbine. When the revolution speed of the rotor increases by the air blow, the speed inevitably passes through the mechanical resonant speed. In the case of the flywheel rotor suspended by the superconducting bearing, there are apparently four fundamental resonant speeds [6, 17]. When the revolution speed of the flywheel rotor reaches one of the speeds, the rotor resonates in self-oscillation. Then the remarkable gyroscopic whirling motion appears and the gap between the PM attached to the rotor and the HTSC changes with the resonant frequency. Therefore, the magnetic field on the surface of the HTSC changes alternatively. Under the magnetic perturbation to the surface of HTSC [12], the levitation force and the gap between the HTSC and PM shows the drift in the same way as in references [9, 10]. The phenomenon does not depend on the HTSC specimen and the dimension of the bulk [18]. However, the mechanism is still not clear.

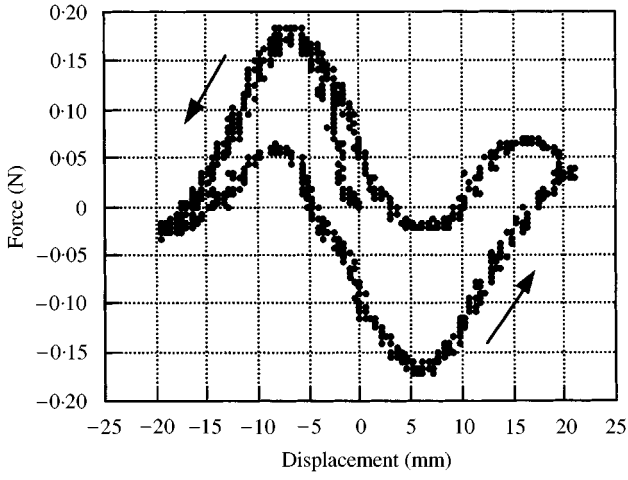

Figure 6. Horizontal force–displacement characteristics.

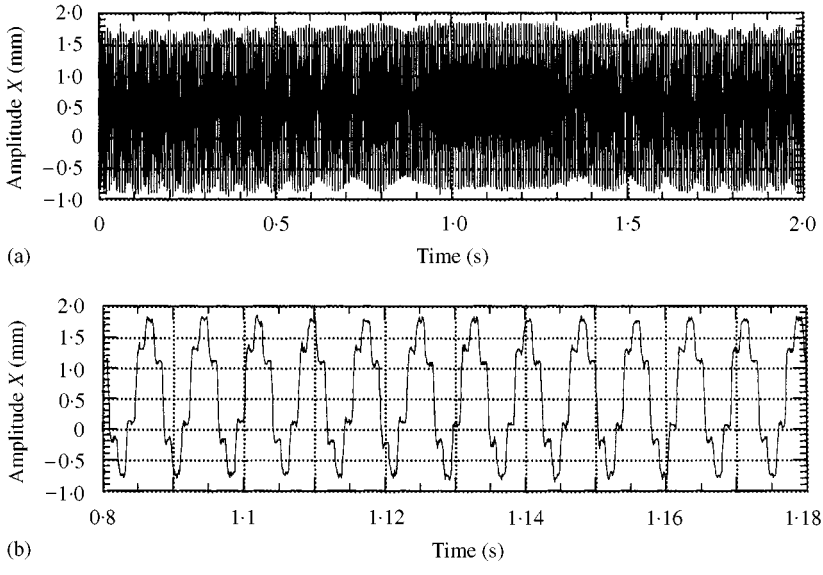

Figure 7. Angular displacement at the decrease of revolution speed, (a) around 8000 r.p.m. (b) extension at 8000 r.p.m.

Under free revolution without air blow, the speed of the rotor decays gradually as a result of the visco resistance of the air and the damping force of the HTSC bearing. Therefore, the revolution speed is swept through the range of the frequency downward automatically. Figure 7(a) shows an angular displacement vibration obtained around 8000 r.p.m. in the x-displacement. The extension of the waveform is given in Figure 7(b). The revolution speed coincides with the harmonic frequencies of the whirling motion when the envelope becomes flat.

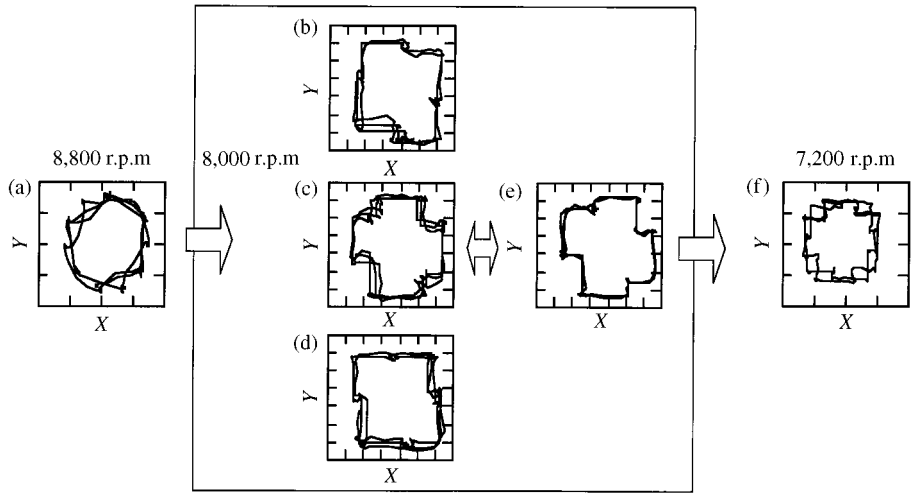

Figure 8. Experimental trajectories of whirling behavior.

Figure 8 shows the experimental trajectories of the whirling motion. At around 8800 r.p.m., the displacement of the flywheel axis shows the trajectory as shown in Figure 8(a). Through the rotation of the state shown in Figure 8(b)–(d), it varies into Figure 8(e). At the state in Figure 8(e), the trajectory keeps the shape while the revolution speed is around 8000 r.p.m. According to the decay of the revolution speed, the trajectory begins to rotate again. Figure 8(f) was obtained at the revolution 7200 r.p.m. In references [2, 3], the appearance of a whirling motion which has similar trajectories was mentioned, but the details were not discussed. The trajectories obtained in this paper seem to be substantial in dynamics affected by the hysteretic suspending force of the HTSC magnetic bearing. Therefore, we will discuss the possibility of the dynamic behavior based on the modelling of the flywheel system in the next section.

4. MATHEMATICAL MODE OF FLYWHEEL ROTOR

The forces working on the rotor suspended by the HTSC magnetic bearing are shown in Figure 9. If there is no damping force, the dynamics of the rotor is given by Euler's equation with the external moment caused by the non-linear hysteretic suspending force between a PM and a HTSC as follows [19]:

$$\frac{\mathrm{d}I_x\omega_x}{\mathrm{d}t} = (I_y - I_z)\,\omega_y\omega_z = M_x,$$

$$\frac{\mathrm{d}I_y\omega_y}{\mathrm{d}t} = (I_z - I_x)\,\omega_z\omega_x = M_y,$$

$$\frac{\mathrm{d}I_z\omega_z}{\mathrm{d}t} = (I_x - I_y)\,\omega_x\omega_y = M_x, \tag{1}$$

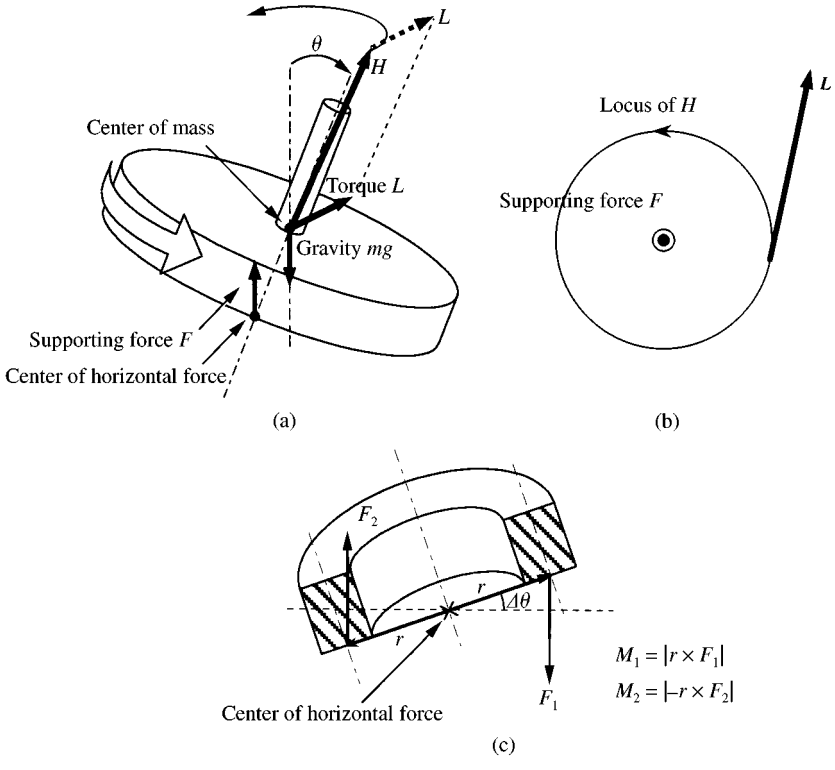

Figure 9. Schematical diagrams of the forces working on the flywheel rotor.

$$\omega_x = \dot{\varphi}\cos\theta\cos\psi + \dot{\theta}\sin\psi,$$
$$\omega_y = \dot{\theta}\cos\psi + \dot{\varphi}\cos\theta\sin\psi,$$
$$\omega_x = \dot{\psi} + \dot{\varphi}\sin\theta, \tag{2}$$

where I_x, I_y and I_z denote the inertia of the rotor, ω_x, ω_y and ω_z the angular velocity, M_x, M_y and M_z the external moment around the x-, y-, zx-axis respectively. (φ, θ, ψ) is the Euler's angular co-ordinate system. The rotor has a cylindrical shape such that $I_x = I_y = I$ and $I_z = J$. Then the moment relationship are approximately given by [6, 20] under the Hamiltonian condition as follows:

$$I(\ddot{\varphi}\cos\theta - \dot{\theta}\dot{\varphi}\sin\theta) + J\dot{\theta}\Omega(1 + \eta\sin\psi) = h_x,$$
$$I(\ddot{\theta} + \dot{\varphi}^2\sin\theta\cos\theta) - J\dot{\varphi}\cos\theta\Omega(1 + \eta\cos\psi) = h_y,$$
$$\dot{\psi} = \Omega - \dot{\varphi}\sin\theta, \tag{3}$$

where η is the sinusoidal amplitude of the inertia around the z-axis, caused by the imbalance of the rotor. We assume that the inertia J changes alternatively depending on the angle ψ around the z-axis. Moreover, h_x and h_y are the external torque around the x- and y-axis respectively. If there is a damping effect in free

revolution, the angular velocity Ω has the following relation:

$$\dot{\Omega} = -\delta\Omega, \tag{4}$$

where δ denotes the damping coefficient of the revolution. The damping mainly depends on the viscodamping of air and magnetic damping of the HTSC magnetic bearing.

On the other hand, the center of mass (x_0, y_0, z_0) has the following relationship:

$$\begin{aligned} m\ddot{x}_0 &= -k(x_0 + \theta z_p), \\ m\ddot{y}_0 &= -k(y_0 - \varphi z_p), \\ m\ddot{z}_0 &= f_{lev}(x, y, z, \varphi, \theta, \psi) - mg, \end{aligned} \tag{5}$$

where k denotes the lateral spring constant, f_{lev} the levitation force working on the rotor and z_p the height of the center of mass from the center of the horizontal force.

Here the external torque h_x and h_y are caused by the hysteretic force between the HTSC and the PM working around the axes. They are approximately represented by

$$\begin{aligned} h_x &= A_1\varphi F_z + A_2\varphi^2 F_x, \\ h_y &= A_1\theta F_z + A_2\theta^2 F_y, \end{aligned} \tag{6}$$

where F_x and F_y denote the lateral force and F_z the vertical force between the HTSC and the PM. A_1 and A_2 can be defined by the dimensions of the rotor. When the angular components φ and θ are small, the torque is approximated by the first terms in equation (6). It implies the vertical force is dominant in the rotational force around the x- and y-axis.

5. MODEL OF HYSTERESIS

In the former section, the force–displacement relation between HTSC and PM was explained based on experimental data. In order to describe the hysteretic characteristics, some numerical models have been proposed [17]. In this paper, a state variable model [8–10, 13, 14] is applied for the vertical force F_z and the lateral force F_x. Based on the model the vertical force–displacement relationship can be well simulated by

$$\begin{aligned} \dot{F}_z &= -\gamma_z \{F_z - f_z(z, \dot{z})\}, \\ f_z(z, \dot{z}) &= f_{z1}(z)\{1 + f_{z2}(\dot{z})\}, \\ f_{z1}(z) &= F_{z0}\, e^{-\beta z}, \\ f_{z2}(\dot{z}) &= \begin{cases} -\mu_1 - \alpha_1\dot{z} & \varepsilon \leqslant \dot{z} \\ -\dot{z}(\mu_1 + \mu_2)/2\varepsilon & -\varepsilon \leqslant \dot{z} < \varepsilon \\ \mu_2 - \alpha_2\dot{z} & \dot{z} < -\varepsilon. \end{cases} \end{aligned} \tag{7}$$

Also, the lateral force–displacement relationship can be simulated by

$$\begin{aligned}
\dot{F}_x &= -\gamma_x\{F_x - f_x(x, \dot{x}, z)\},\\
f_x(x, \dot{x}, z) &= f_{x0}(x)\,\{f_{x1}(x, z) - f_{x2}(\dot{x}, z)\},\\
f_{x0}(x) &= F_{x0}\,\mathrm{e}^{-\sigma x^2},\\
f_{x1}(x, z) &= f_{z1}(z)\,(x^3 - x),\\
f_{x2}(\dot{x}, z) &= \begin{cases} -\xi_1 \mathrm{e}^{-\beta z} & \varepsilon \leqslant \dot{x}\\ -(\xi_1/\varepsilon)\,\dot{x}\mathrm{e}^{-\beta z} & -\varepsilon \leqslant \dot{x} < \varepsilon\\ \xi_1\,\mathrm{e}^{-\beta z} & \dot{z} < -\varepsilon. \end{cases}
\end{aligned} \tag{8}$$

These models can represent the shapes of major one-dimensional hysteretic characteristics as shown in Figure 10 and 11. The parameters are given in Table 1. They are closely similar to the experimental results as shown in Figures 5 and 6 [9, 10]. It is easy to include the model into the dynamical equation of the flywheel rotor, which was obtained in the section 4.

6. NUMERICAL SIMULATIONS OF ROTOR DYNAMICS

The dynamics of the flywheel rotor under free revolution can be simulated based on the above-mentioned mathematical equations. When the revolution speed decays gradually depending on the damping effect, the self-excited vibration is induced by the revolution.

6.1. SYSTEM PARAMETERS

The flywheel rotor system described by differential equations (3) and (4) has the non-linear characteristics both in the force–displacement relationship and in the

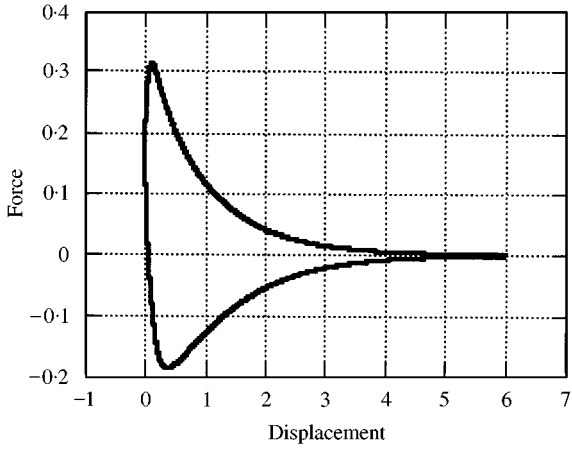

Figure 10. Vertical force–displacement hysteresis.

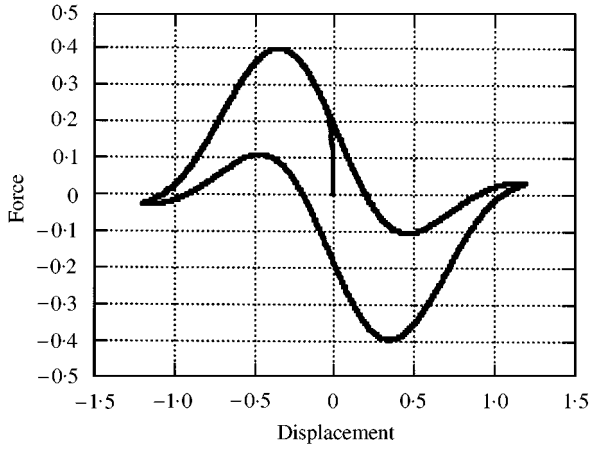

Figure 11. Lateral force–displacement hysteresis.

TABLE 1

Paramter settings

Parameter	Value	Unit
I	$3{\cdot}911 \times 10^{-4}$	kg m^2
J	$2{\cdot}153 \times 10^{-4}$	kg m^2
k	2700	N/m
m	0·456	kg
z_p	$-1{\cdot}12 \times 10^{-2}$	m
A_1	0·4370	N/m/rad
γ_z	0·085	
F_{z0}	0·2	
β	0·82	
μ_1	− 1·8	
μ_2	− 0·2	
ε	0·01	
α_1	− 2·0	
α_2	0·0	
η	0·01	
γ_x	1·0	
F_{x0}	1·0	
σ	2·0	
x_i	0·2	
δ	$5{\cdot}0 \times 10^{-4}$	

rigid-body dynamical relationship depending on the angular factor. Therefore, the imbalance of the rotor and the initial position possibly cause the complicated dynamic behaviour. If the rotor does not have any contact with their support, it is free from the friction damping. However, the hysteretic characteristics of the HTSC bearing causes the hysteresis energy loss and the damping of the vibration when the

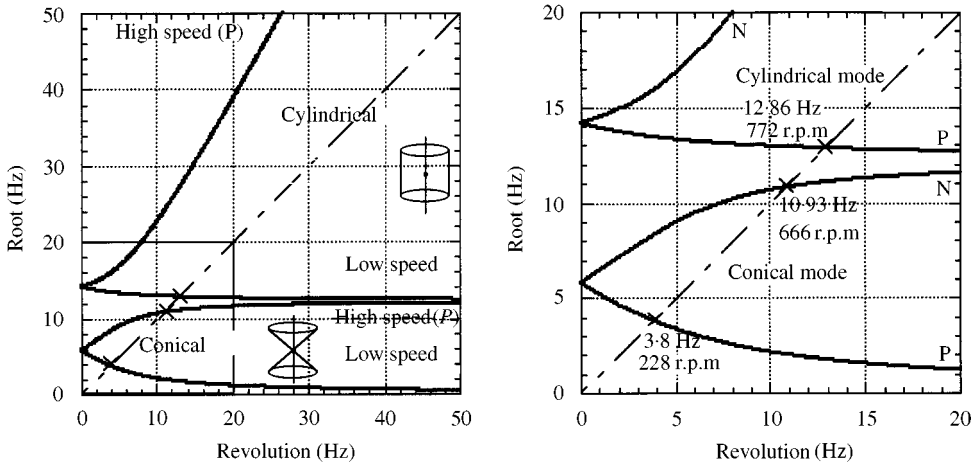

Figure 12. Resonant frequencies in gyroscopic behavior.

magnetic field varies on the surface of HTSC specimens. In this numerical simulations, the parameters in the equations are also fixed as shown in Table 1. They are adjusted to the flywheel system in this experiment quantitatively.

6.2. GYROSCOPIC BEHAVIOR

The linear analysis of the flywheel rotor model gives us the resonant frequency caused by the gyroscopic dynamics. There are four fundamental resonant frequencies. They are shown in Figure 12. The cross-points of the resonant frequencies and the driving curve (broken line) imply the fundamental resonant frequencies. They are lower than 12·86 Hz (772 r.p.m.). There are other possibilities of the subresonance at the higher order subresonant mode. However, in experiments these possibilities are not confirmed.

6.3. DYNAMIC BEHAVIOR

When the revolution speed of the rotor passes through the resonant frequencies of the whilring motion, the trajectory shows the simple oval locus. In order to confirm the whirling behaviour in simulation, the free downward revolution are given under the damped state. The initial position of the rotor was set at $(\varphi, \theta, \psi) = (0{\cdot}0001, 0, 0)$ and the velocity at $(\dot{\varphi}, \dot{\theta}, \dot{\psi}) = (0, 0, 0)$.

Figure 13 shows the simulated vibration of φ versus the decreasing revolution speed under the free downward revolution. The waveform of angular displacement around 8800 r.p.m. (148 Hz) includes the distortion. It seems to depend on the non-linearity of the system, especially the hysteretic suspending force. At some revolution speed the waveform was kept during the whirling motion as we have seen in experiments.

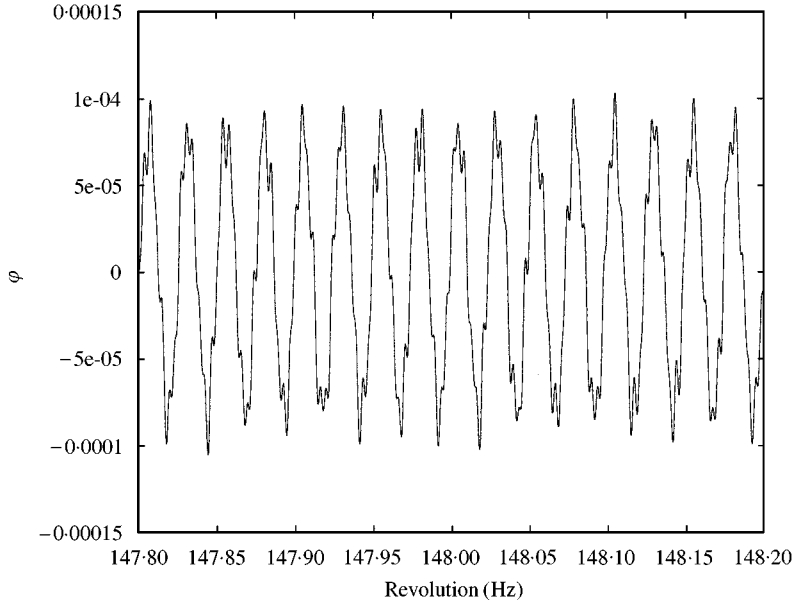

Figure 13. Vibration of Euler angle φ versus revolution speed around 148 Hz (8880 r.p.m.).

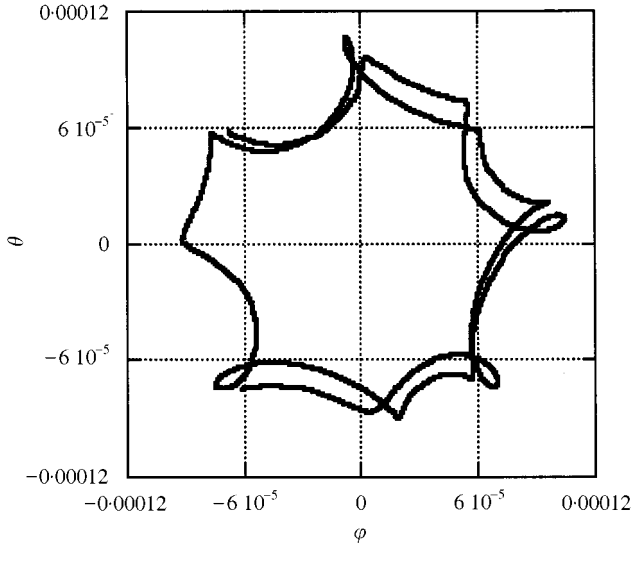

Figure 14. Simulation trajectory of Euler angle on φ–θ plane at 148·1 Hz (8886 r.p.m.).

Figures 14 shows the trajectory of (φ, θ) at 8886 r.p.m. Before and after the state in Figure 13, the whirling motion changes the direction of the rotation from forward to backward. The phenomenon is similar to the experimental results. Moreover, the trajectory is very similar to the experimental results in its shape. That is, the cross-like shaped trajectory appears without any special condition for

the trajectory. It depends mainly on the hysteretic force–displacement relationship between the HTSC and the PM. If the force has no hysteretic characteristics, it is easily confirmed that the trajectories of the whilring motion become a simple oval. Therefore, the hysteretic characteristic of the HTSC magnetic bearings are substantial in the modelling of the whilring behavior of the HTSC flywheel system. Moreover, the model is highly advantageous in substituting itself into the differential equations for describing the dynamics.

7. CONCLUSIONS

The flywheel rotor suspended by the HTSC magnetic bearing shows interesting dynamic behavior. It was experimentally shown that the whirling motion at a high revolution speed showed the cross-shaped trajectory. The trajectory greatly depends on the hysteretic force–displacement relationship between the HTSC and the PM in the bearing system. In order to realize the dynamics of the flywheel rotor at a high revolution speed, a mathematical model was proposed. As a result, the numerical simulation also shows the appearance of the trajectories which are observed in experiments, when the hysteretic force relation is considered.

In the development of the HTSC energy storage system, the technical discussion is liable to precede the fundamental theoretical one. However, the experimental results obtained in the prototype system sometimes reveal the substantial physical feature of the non-linear system. It must be considered that the hysteretic characteristics between the HTSC and the PM have an important role in the dynamic behavior, when the dynamics is intended to be controlled. Moreover, the rigid-body dynamics with the hysteretic suspending force has never been considered before. The results obtained in this paper give us much information about such new types of problems.

ACKNOWLEDGMENTS

The authors would like to acknowledge the experimental support of Professor Y. Hirane and Dr. S. Ohashi of Kansai University.

REFERENCES

1. F. C. Moon and P.-Z. Chang, 1990 *Applied Physics Letter* **56**, 397–399. High-speed rotation of magnets on high Tc superconducting bearings.
2. R. Takahata and H. Ueyama 1991 *Proceeding of the Fourth International Symposium on Superconductor* 1089–1092. Characterization of superconducting magnetic bearings (vibration damping and hysteresis of magnetic force in superconductor).
3. H. Takaichi and *et al.* 1992 *Proceedings of the Third International Symposium of Magnetic Bearings* 307–316. The application of bulk YBaCuO for a practical superconducting magnetic bearing.
4. J. T. Harding and D. B. Lawson 1968 *AIAA Journal* **6**, 305. Method for rapidly reversing magnetic field in shorted superconducting coil.
5. J. T. Harding 1966 *Review of Scientific Instruments* **37**, 1350. Superconducting gyroscope: drift data and mathematical model.

6. R. D. Bourke 1969 *NASA CR*-108. A theoretical and experimental study of a superconducting magnetically-supported spinning body.
7. A. N. Terentiev and A. A. Kuzunetsov 1992 *Physica C* **195**, 41–46. Drift of levitated YBCO superconductor induced by both a variable magnetic field and a vibration.
8. T. Hikihara and F. C. Moon 1994 *Physics Letters A* **191**, 279–284. Chaotic levitation motion of a magnet supported by superconductor.
9. T. Hikihara and F. C. Moon 1995 *Physica C*, **250**, 121–127. Levitation drift of a magnet supported by a high-Tc superconductor under vibration.
10. T. Hikihara and G. Isozumi 1996 *Physica C* **270**, 68–74. Modelling of lateral force-displacement hysteresis caused by local flux pinning.
11. T. A. Coombs and A. M. Campbell 1996 *Physica C* **256**, 298–301. Gap decay in superconducting magnetic bearings under the influence of vibration.
12. T. Hikihara, H. Adachi, S. Ohashi, Y. Hirane and Y. Ueda, 1997 *Physica C*, **291**, 34–40. Levitation drift of flywheel and HTSC bearing system caused by mechanical resonance.
13. T. Hikihara and Y. Ueda 1997 *International Symposium of Nonlinear Electromagnetic Systems. ISEM-Braunschweig*, *Germany* May 12–14. A dynamical model of high speed rotor suspended by high-Tc superconducting bearing.
14. T. Hikihara, F. C. Moon and Y. Ueda 1998 *LDIA*'98 *Tokyo*, *Japan* April 8–10. A study on dynamics of flywheel rotor suspended by high-Tc superconducting bearing.
15. P. Schönhuber and F. C. Moon 1994 *Applied Superconductivity* **2**, 523–534. Levitation forces, stiffness and force-creep in YBCO high-Tc superconducting thin films.
16. H. Hashizume, T. Sugiura, K. Miya and S. Toda 1992 *IEEE Transaction on Magnetics*, **28**, 1332–1335. Numerical analysis of electromagnetic phenomena in superconductors.
17. F. C. Moon 1993 *Superconducting Levitation.* New York: Wiley.
18. S. Ohashi, Y. Hirane and T. Hikihara *Inter Mag* '99, *Korea.* Three-dimensional vibration of the rotor in the HTSC-permanent magnet flywheel system. (submitted).
19. D. T. Greenwood 1998 *Principles of Dynamics*, Section 2 edition. Englewood Cliff, NJ: Prentice-Hall.
20. T. Hikihara 1995 *Technical Report of IEICE*, NLP95-35 (in Japanese). Dynamics of rotating body suspended by HTSC bearing.
21. T. Hikihara and F. C. Moon 1994 *Cornell University Report*. Numerical studies on dynamical behavior of high speed rotor supported by high Tc superconducting bearing.